Rephasing processes and quantum memory for light: reversibility issues and how to fix them

2012 J. Phys. B: At. Mol. Opt. Phys. 45 124003

(http://iopscience.iop.org/0953-4075/45/12/124003)

J. Phys. B: At. Mol. Opt. Phys. **45** (2012) 124003 (7pp) doi:10.1088/0953-4075/45/12/124003

Rephasing processes and quantum memory for light: reversibility issues and how to fix them

Sergey A Moiseev[1,2] **and J-L Le Gouët**[3]

[1] Kazan Physical-Technical Institute of the Russian Academy of Sciences,10/7 Sibirsky Trakt, Kazan, 420029, Russia
[2] Institute for Informatics of Tatarstan Academy of Sciences, 20 Mushtary, Kazan, 420012, Russia
[3] Laboratoire Aimé Cotton, CNRS-UPR 3321, Université Paris-Sud, Bât 505, 91405 Orsay Cedex, France

E-mail: samoi@yandex.ru and jean-louis.legouet@lac.u-psud.fr

Received 31 August 2011, in final form 24 November 2011
Published 8 June 2012
Online at stacks.iop.org/JPhysB/45/124003

Abstract
Time reversibility has been absent from some recently proposed quantum memory protocols such as the atomic frequency comb (AFC) scheme. Focusing on AFC memory, we show that quantum efficiency and fidelity are reduced dramatically, as a consequence of non-reversibility, when the spectral width of the incoming signal approaches the memory bandwidth. Non-reversibility is revealed through spectral dispersion, giving rise to phase mismatching. We propose a modified AFC scheme that restores reversibility. This way, signals can be retrieved with excellent efficiency over the entire memory bandwidth. This study could be extended to other quantum memory rephasing schemes in inhomogeneously broadened absorbing media.

(Some figures may appear in colour only in the online journal)

1. Introduction

Rephasing processes in inhomogeneously broadened absorption lines [1–3] offer an attractive way to store and retrieve a large number of optically carried temporal modes [4–7]. This property raises increasing interest in the quest for multi-mode quantum memories (QMs) for light [8–10].

In the first proposed rephasing QM scheme, known as controlled reversible inhomogeneous broadening (CRIB) [11–14], the retrieval step is devised to be the exact time reversed copy of the storage phase. Perfect reversibility is preserved even with broadband signals spanning the entire absorption line, provided all the incoming spectral components are completely captured in the memory material. The required inhomogeneous broadening is generated by an external electric field through the Stark effect. The frequency detuning is reversed by Stark switching. Hence, atomic coherences can be brought back in phase together and are able to restore the original signal. To satisfy the time and space symmetry requirement, the signal must be recovered in the backward direction, where efficiency can reach 100%. To this end, the initially excited coherences have to be converted into spin or hyperfine coherences and back. In the forward direction, retrieval efficiency drops to about 54%.

The practical implementation of CRIB led to the emergence of a novel scheme, known as gradient echo memory (GEM) [15–17], where the absorption line is *not* inhomogeneously broadened *locally*. Instead, inhomogeneous broadening only appears through integration over the material depth. With GEM, 100% efficiency is expected in the forward direction, in spite of imperfect reversibility. Actually, record quantum efficiency (QE) has been reported recently in solid [18] and gaseous [19] media. The lack of reversibility is revealed by fidelity reduction [16, 20]. Experimentally, with retrieval in the forward direction, one no longer needs ancillary spin or hyperfine coherences, as in CRIB. Hence, GEM works with two-level atoms.

Alternative rephasing techniques have been proposed recently [21–25]. They avoid the frequency detuning reversal step. Among those new protocols, atomic frequency combs (AFC) have already given rise to a large harvest of promising experimental results. In AFC-based memories, the signal is captured by an evenly spaced spectral array of absorption teeth. As a result, coherences are automatically phased back

together after a delay given by the inverse spacing of the absorption teeth. In contrast with CRIB, the revival step is not time reversed with respect to the storage step. Actually, the signal is restored with the same time order as the original one. Using AFC, a much wider bandwidth with a much larger temporal multi-mode capacity has been demonstrated than with CRIB and GEM [26, 27]. In addition, for the first time in a solid, storage and retrieval of photonic entanglement have been demonstrated using AFC [28, 29]. However, those results have been obtained with rather modest QE, presumably because of practical difficulties in the absorption tooth array preparation.

Beyond practical limitations, one should question the lack of temporal symmetry or reversibility in the latter processes. In this paper, we examine this question in the specific case of AFC-based memories. In section 2, we consider the capture of an incoming quantum field by a finite-bandwidth AFC. In section 3, we express the recovered signal and analyze the negative impact of dispersion effects on AFC QE and fidelity. We also delineate the difference between CRIB and AFC regarding reversibility. In section 4, in the light of this analysis, we propose a modified AFC (MAFC) scheme providing almost 100% QE and perfect fidelity over the whole spectral range of the AFC filter. Finally, we briefly consider the extension of this method to other non-reversible QM for light protocols.

2. Capturing the incoming signal

Following the basic scheme of photon echo QM, we consider an ensemble of N three-level atoms initially prepared in the ground state $|1\rangle = \prod_{j=1}^{N} |1\rangle_j$. The optical transition at frequency $\omega_{12;j}$ to the upper level $|2\rangle_j$ is excited by the signal field $\mathbf{A}_p(\tau, z)$. The quantum dynamics of the light–matter system is described by linearized Maxwell–Bloch equations. In the weak field limit, the jth atom coherence $\mathbf{S}(\tau, \Delta_j, z_j) = |1\rangle_{jj}\langle 2|$ obeys the equation

$$\partial_\tau \mathbf{S}(\tau, \Delta_j, z) = -\mathrm{i}(\omega_o + \Delta_j)\mathbf{S}(\tau, \Delta_j, z) + \mathrm{i}g\mathbf{A}_p(\tau, z)\exp\{-\mathrm{i}\omega_p\tau\}, \quad (1)$$

where ω_o, ω_p and $\Delta_j = \omega_{12;j} - \omega_o$ respectively denote the atomic transition central frequency, the signal field carrier frequency and the jth atom detuning from the central frequency. Time in the moving frame is represented by $\tau = t - z/c$. The photon–atom coupling constant is defined as $g = \mathrm{i}\wp\sqrt{\omega_o/2\hbar\varepsilon_o S_o}$, where $\wp$, ε_o and $\hbar$ respectively stand for the atomic transition dipole moment, the electric permittivity and the Planck constant divided by 2π. Throughout the paper we neglect the coherence decay, assuming the experiment timescale to be much shorter than the coherence lifetime. The radiative reaction of the atoms to electromagnetic excitation is expressed at a macroscopic level, involving the average over many atoms and substituting a continuous medium to the discrete atom distribution. This scale change is mediated by the macroscopic coherence

$$\mathbf{S}(\tau, z) = \int \mathrm{d}\Delta C(\Delta)\mathbf{S}(\tau, \Delta, z), \quad (2)$$

where the average at position z is performed over the transition frequency distribution $C(\Delta)$, centred at $\Delta = 0$. The light field propagation is then described by

$$\partial_z \mathbf{A}_p(\tau, z) = \mathrm{i}\beta\exp\{\mathrm{i}\omega_p\tau\}\mathbf{S}(\tau, z), \quad (3)$$

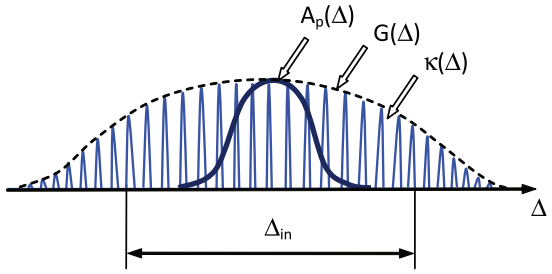

Figure 1. AFC filter $C(\Delta)$ uniformly engraved over the entire width of an inhomogeneously broadened absorption line $G(\Delta)$. The initial inhomogeneous width, the absorption tooth profile and the incoming signal spectrum are respectively denoted as Δ_{in}, $\kappa(\Delta)$ and $A_p(\Delta)$.

where $\beta = \pi(n_o S_o)(g^*/c)$ is the function of the atomic concentration n_o, the light-beam cross section S_o and the photon–atom coupling constant.

Let us consider an ideal AFC structure, uniformly engraved over the entire available inhomogeneous width, as depicted in figure 1:

$$C(\Delta) = \frac{1}{\kappa(0)\delta}\left[\text{Ш}\left(\frac{\Delta}{\delta}\right) * \kappa(\Delta)\right] G(\Delta), \quad (4)$$

where $\text{Ш}(x) = \sum_n \delta(x - n)$ represents a Dirac comb, $*$ is a convolution symbol, $\kappa(\Delta)$ stands for the profile of each comb tooth. According to the $\text{Ш}(x)$ definition, δ in equation (4) denotes the tooth spacing. The widths of $G(\Delta)$ and $\kappa(\Delta)$ are denoted Δ_{in} and b, respectively. They satisfy the condition $b \ll \delta \ll \Delta_{\mathrm{in}}$. Both $G(\Delta)$ and $\kappa(\Delta)$ are normalized according to

$$\int G(\Delta)\mathrm{d}\Delta = \int \kappa(\Delta)\,\mathrm{d}\Delta = 1. \quad (5)$$

The normalization factor $[\kappa(0)\delta]^{-1} \approx b/\delta$ makes $C(\Delta)$ coincide with the initial distribution $G(\Delta)$ at the top of the comb teeth. Solving the Bloch equation (1) and summing over Δ, one obtains

$$\mathbf{S}(\tau, z) = \mathrm{i}g\mathrm{e}^{-\mathrm{i}\omega_p\tau}\int_{-\infty}^{\tau}\mathrm{d}\tau'\mathbf{A}_p(\tau', z)\int \mathrm{d}\Delta C(\Delta)\mathrm{e}^{-\mathrm{i}\Delta(\tau-\tau')}. \quad (6)$$

The Dirac comb satisfies the Fourier transform property

$$\int \mathrm{d}x\,\text{Ш}(x)\,\mathrm{e}^{-\mathrm{i}xu} = \text{Ш}\left(\frac{u}{2\pi}\right). \quad (7)$$

Therefore,

$$\int \mathrm{d}\Delta C(\Delta)\,\mathrm{e}^{-\mathrm{i}\Delta t} = \frac{1}{\kappa(0)\delta}\sum_n \tilde{\kappa}\left(\frac{2\pi n}{\delta}\right)\tilde{G}\left(t - \frac{2\pi n}{\delta}\right), \quad (8)$$

where $\tilde{f}(t) = \int \mathrm{d}\Delta f(\Delta)\mathrm{e}^{-\mathrm{i}\Delta t}$. Substitution into equation (6) leads to

$$\mathbf{S}(\tau, z) = \sum_n \mathbf{S}^{(n)}(\tau, z), \quad (9)$$

where

$$\mathbf{S}^{(n)}(\tau, z) = \mathrm{i}g\mathrm{e}^{-\mathrm{i}\omega_p\tau}\frac{1}{\kappa(0)\delta}\tilde{\kappa}\left(\frac{2\pi n}{\delta}\right) \times \int_0^{\infty}\mathrm{d}\tau'\mathbf{A}_p(\tau - \tau', z)\tilde{G}\left(\tau' - \frac{2\pi n}{\delta}\right). \quad (10)$$

Because of causality, expressed by the lower boundary in the integral, the sum runs over positive n values only.

According to this expression, the macroscopic coherence revives periodically, with $2\pi/\delta$ time intervals.

If the incoming signal is much shorter than $2\pi/\delta$, the n-indexed terms do not overlap. Each represents the coherence revival at time $2n\pi/\delta$. The $n = 0$ term is involved in the instantaneous signal propagation. Then, equation (3) reduces to

$$\partial_z \mathbf{A}_p(\tau, z) = -\frac{\beta g}{\kappa(0)\delta}\int_0^\infty \mathrm{d}\tau' \mathbf{A}_p(\tau-\tau', z)\tilde{G}(\tau'), \quad (11)$$

where we have replaced $\tilde{\kappa}(0)$ par 1, in accordance with the normalization condition, and we have dropped the $\mathrm{e}^{-\mathrm{i}(\omega_o-\omega_p)\tau'}$ factor, very close to unity (i.e. $\omega_o \cong \omega_p$). The spectral amplitude defined as $\tilde{\mathbf{A}}_p(\omega, z) = \int_{-\infty}^{\infty}\mathrm{d}\tau \mathbf{A}_p(\tau, z)\exp\{\mathrm{i}\omega\tau\}$ satisfies the familiar equation

$$\partial_z \tilde{\mathbf{A}}_p(\omega, z) + \mathrm{i}\frac{\omega_p}{2c}\chi(\omega)\tilde{\mathbf{A}}_p(\omega, z) = 0, \quad (12)$$

where the real and imaginary parts of susceptibility $\chi(\omega)$ respectively read

$$\chi'(\omega) = \frac{c}{\omega_p}\alpha(0)\frac{1}{\pi}\mathrm{P}\int_{-\infty}^{\infty}\frac{G(\Delta)/G(0)}{\omega-\Delta}\mathrm{d}\Delta, \quad (13)$$

$$\chi''(\omega) = -\frac{c}{\omega_p}\alpha(\omega), \quad (14)$$

where P denotes the Cauchy principal value and the linear absorption coefficient is given by

$$\alpha(\omega) = \frac{2\pi\beta g}{\kappa(0)\delta}G(\omega). \quad (15)$$

One easily solves equation (12) as

$$\tilde{\mathbf{A}}_p(\omega, z) = \exp\left\{-\mathrm{i}\frac{\omega_p}{2c}\chi(\omega)z\right\}\tilde{\mathbf{A}}_p(\omega, 0).$$

With respect to the initial atomic distribution, the absorption coefficient is modified by the factor $[\kappa(0)\delta]^{-1} \approx b/\delta$. When $G(\Delta)$ is symmetric, $\chi'(0) = 0$ and $|\chi'(\omega)|$ increases almost linearly for $|\omega|/\Delta_{\mathrm{in}} \leqslant 1$.

Contemplating equations (12)–(14), one must remember that they rely on the assumption that the incoming signal spectrum is much broader than the absorbing comb spacing. Hence $\chi(\omega)$, representing a coarse graining approximation of the comb susceptibility, is expressed in terms of the AFC envelope $G(\Delta)$. Then $\chi(\omega)$ exhibits the features of an absorption line, with abnormal dispersion within the absorption profile. Should the absorption coefficient $\omega_p\chi''(\omega)/c$ be large enough, this may result in negative group velocity and so-called superluminal propagation [30].

As an illustration, let both $G(\Delta)$ and $\kappa(\Delta)$ be given a Gaussian profile according to

$$G(\Delta) = \sqrt{\frac{\zeta}{\pi}}\frac{1}{\Delta_{\mathrm{in}}}\exp\left(-\zeta\frac{\Delta^2}{\Delta_{\mathrm{in}}^2}\right)$$

$$\kappa(\Delta) = \sqrt{\frac{\zeta}{\pi}}\frac{1}{b}\exp\left(-\zeta\frac{\Delta^2}{b^2}\right),$$

where $\zeta = 4\mathrm{Ln}(2)$ and Δ_{in} and b stand for the full-width at half-maximum (FWHM) of the respective shapes. Assuming $\delta \gg b$, substitution into equations (13) and (14) leads to

$$\chi'(\omega) = -\frac{c}{\omega_p}\alpha_o\exp\left(-\zeta\frac{\omega^2}{\Delta_{\mathrm{in}}^2}\right)\mathrm{Erfi}\left(-\sqrt{\zeta}\frac{\omega}{\Delta_{\mathrm{in}}}\right)$$

and

$$\chi''(\omega) = -\frac{c}{\omega_p}\alpha_o\exp\left(-\zeta\frac{\omega^2}{\Delta_{\mathrm{in}}^2}\right),$$

where $\alpha_o = \frac{2\pi b}{\delta}\frac{\beta g}{\Delta_{\mathrm{in}}}$. Absorption equals dispersion at $|\omega/\Delta_{\mathrm{in}}| = 0.425$, which points out the importance of dispersion effects when the signal spectral width approaches the AFC bandwidth.

3. Signal recovery

As already pointed out, the macroscopic coherence revives periodically, giving rise to delayed responses. In the framework of filtering by an infinitely broad AFC, an exact replica of the incoming signal can be retrieved in the backward direction at time $2\pi/\delta$ with 100% efficiency [22]. This way, AFC storage appears to be perfectly reversible. Emission in the backward direction involves two counterpropagating π-pulses. They convert the optical atomic coherence into a long-lived coherence and back, extending the storage time well beyond $2\pi/\delta$. When restored by the second π-pulse, the optical coherence phase has been changed by $2kz$, which causes emission in the backward direction. In the case of CRIB, perfect reversibility in the backward direction can be achieved without the restriction of an infinitely broad processing bandwidth [31]. We precisely aim at clarifying this point in the case of AFC.

Following the lines of [22, 31], we restrict the discussion to the backward retrieval scheme. Let $\mathbf{A}_r(\tilde{\tau}, z)$ represent the retrieved field in terms of the new moving frame coordinates $\tilde{\tau} = t + z/c$, $z = z$. In this frame, the field equation reads

$$-\tfrac{\partial}{\partial z}\mathbf{A}_r(\tilde{\tau}, z) = \mathrm{i}\beta\exp\{\mathrm{i}\omega_o\tilde{\tau}\}\mathbf{S}(\tilde{\tau}, z), \quad (16)$$

where $\mathbf{S}(\tilde{\tau}, z)$ is comprised of the first revival of the atomic coherence previously excited by the signal field, and of the instantaneous response of the medium to the retrieved field. Components $\mathbf{S}^{(1)}(\tilde{\tau}, z)$ and $\mathbf{S}^{(0)}(\tilde{\tau}, z)$, as defined in equation (10), respectively describe those two contributions. Substitution into equation (16) leads to

$$-\tfrac{\partial}{\partial z}\tilde{\mathbf{A}}_r(\omega, z) = \tfrac{\omega_p}{2c}\{\mathrm{i}\chi(\omega)\tilde{\mathbf{A}}_r(\omega, z) + 2\tilde{\kappa}(2\pi/\delta)\chi''(\omega)\tilde{\mathbf{A}}_p(\omega, z)\}. \quad (17)$$

Solving in z and Fourier transforming back to the time domain lead to the retrieved field expression at the medium output, i.e. in the front side at $z = 0$:

$$\mathbf{A}_r(\tilde{\tau}, 0) = \tilde{\kappa}(2\pi/\delta)\int_{-\infty}^{\infty}\frac{\mathrm{d}\omega}{2\pi}\Gamma(\omega)\tilde{\mathbf{A}}_p(\omega, 0)\exp(-\mathrm{i}\omega\tilde{\tau}), \quad (18)$$

where the complex efficiency $\Gamma(\omega)$ reads

$$\Gamma(\omega) = \frac{1-\exp[\mathrm{i}\omega_p\chi(\omega)L/c]}{\{1-\mathrm{i}\chi'(\omega)/\chi''(\omega)\}}. \quad (19)$$

With absorption teeth being much narrower than their spacing, $\tilde{\kappa}(2\pi/\delta)$ is close to 1. Further assuming $G(\Delta)$ to be continuous, one can make factor $\{1-\exp[\mathrm{i}\frac{\omega}{c}\chi(\omega)L]\}$ arbitrarily close to 1 over the signal spectral range by increasing the medium thickness L. Still the signal is not recovered with 100% efficiency.

The frequency-dependent weight factor $1/[1 - i\chi'(\omega)/\chi''(\omega)]$ distorts and depletes the retrieved signal. The quantity $\chi'(\omega)/\chi''(\omega)$ represents nothing but the spatial phase mismatching that builds up over a round trip in the medium, down to the inverse absorption coefficient corresponding to the penetration depth. All the spectral components are depleted independently. Indeed, the phase mismatch builds up between the atoms and the signal field, at each frequency.

At this stage, the difference with CRIB can be clearly understood. In AFC-based memory, the part of information in channel ω that is captured at depth z undergoes the frequency-dependent $\omega_p\chi'(\omega)z/c$ phase shift, down to the storage position. The same phase shift is accumulated on the way back to the input surface when the signal is restored, which doubles the phase shift. In CRIB, the same superluminal feature takes place. However, information captured in channel ω is transferred to channel $-\omega$ when the frequency detuning is reversed. Hence, because $\chi'(\omega)$ is an odd function of ω, the information initially captured at ω, and retrieved at $-\omega$, undergoes phase shift $-\omega_p\chi'(\omega)z/c$ on the way back to the material surface, which cancels the phase shift accumulated on the way in [31]. This is made possible because the detuning reversal does not affect propagation. Hence, the susceptibility remains unchanged throughout the process.

Despite the non-reversibility of AFC-based memory, the phase shift vanishes in the infinitely broad AFC limit considered in previous works. However, retrieval may be significantly altered when the signal bandwidth becomes similar to the AFC width. Indeed, $\chi'(\omega)/\chi''(\omega)$ variation over the AFC spectrum may exceed unity. For instance, in the frame of the previously considered AFC Gaussian envelope, $\chi'(\omega)/\chi''(\omega) \cong \rho\omega/\Delta_{\text{in}}$ for $|\omega|/\Delta_{\text{in}} < 1$, with $\rho \cong 1.385$. Then, $\chi'(\omega)$ equals $\chi''(\omega)$ at $|\omega/\Delta_{\text{in}}| = 0.425$. This may strongly affect both the QE and fidelity, as discussed in the following.

3.1. Quantum efficiency

The memory QE is defined as

$$Q = \frac{\int_{-\infty}^{\infty} \mathrm{d}\omega \langle \tilde{\mathbf{A}}_r^+(\omega, 0)\tilde{\mathbf{A}}_r(\omega, 0)\rangle}{\int_{-\infty}^{\infty} \mathrm{d}\omega \langle \tilde{\mathbf{A}}_p^+(\omega, 0)\tilde{\mathbf{A}}_p(\omega, 0)\rangle}, \tag{20}$$

where quantum averaging is performed over the initial state of the light field. The spectral density of the input light intensity can be expressed as $I_p(\omega) = \left\langle \tilde{\mathbf{A}}_p^+(\omega, 0)\tilde{\mathbf{A}}_p(\omega, 0)\right\rangle$. Then, substitution of equations (18) and (19) into equation (20) leads to

$$Q = [\tilde{\kappa}(2\pi/\delta)]^2\tilde{Q}, \tag{21}$$

where

$$\tilde{Q} = \int_{-\infty}^{\infty} \mathrm{d}\omega |\Gamma(\omega)|^2 I_p(\omega) \Big/ \int_{-\infty}^{\infty} \mathrm{d}\omega\, I_p(\omega). \tag{22}$$

QE critically depends on the narrowness of the absorbing teeth through factor $[\tilde{\kappa}(2\pi/\delta)]^2$ that approaches 1 when $b \ll \delta$.

As an illustration, let a Gaussian-shaped signal $I_p(\omega) = I_p(0)\sqrt{\frac{\zeta}{\pi}}\frac{1}{\Delta_p}\exp\left(-\zeta\frac{\omega^2}{\Delta_p^2}\right)$ be captured through the previously considered Gaussian-shaped AFC. Under assumption of infinite optical depth, QE can be expressed for $\Delta_p/\Delta_{\text{in}} < 1$ as

$$Q_G = \frac{[\tilde{\kappa}(2\pi/\delta)]^2\sqrt{\pi/2}}{0.9|\Delta_p/\Delta_{\text{in}}|}\exp\left\{\frac{1}{2(0.9\Delta_p/\Delta_{\text{in}})^2}\right\} \times \mathrm{Erfc}\left\{\frac{1}{0.9\sqrt{2}|\Delta_p/\Delta_{\text{in}}|}\right\}. \tag{23}$$

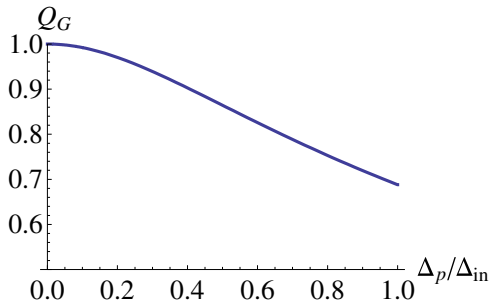

Figure 2. QE Q_G as a function of relative bandwidth $\Delta_p/\Delta_{\text{in}}$ when both the AFC and the captured signal are Gaussian shaped. Atomic decoherence is ignored and the optical depth is infinite.

The corresponding QE is plotted in figure 2 as a function of the relative bandwidth $\Delta_p/\Delta_{\text{in}}$. It shows that QE drops below 90% when the signal bandwidth exceeds 0.4 times the AFC width. The decrease can be even stronger for different spectral shapes, such as a Lorentzian.

The extension to multiple temporal mode storage is straightforward when the different temporal modes do not overlap. Then multi-mode QE coincides with the single-mode efficiency, provided the comb shape does not change during the capture of the mode train.

3.2. Fidelity

The memory fidelity is expressed in terms of the output state projection on the input state. Let the signal field be prepared in a single photon state

$$|\psi_{\text{in}}(t)\rangle = \int_{-\infty}^{\infty} \mathrm{d}\omega f_p(\omega)\exp\{-i\omega t\}\mathbf{a}^+(\omega)\,|0\rangle, \tag{24}$$

where the creation and annihilation operators $\mathbf{a}^+(\omega)$ and $\mathbf{a}(\omega')$ obey the commutation relation $[\mathbf{a}(\omega'), \mathbf{a}^+(\omega)] = \delta(\omega - \omega')$, and where the spectral distribution $f_p(\omega)$ satisfies the normalization condition

$$\int_{-\infty}^{\infty} \mathrm{d}\omega |f_p(\omega)|^2 = 1.$$

The normalized output state can be derived from equation (18) as

$$|\psi_{\text{out}}(t)\rangle = \int_{-\infty}^{\infty} \mathrm{d}\omega\Gamma(\omega)f_p(\omega)\exp[-i\omega(t - T)]\mathbf{a}^+(\omega)\,|0\rangle \Big/ \left[\int_{-\infty}^{\infty} \mathrm{d}\omega|\Gamma(\omega)f_p(\omega)|^2\right]^{1/2}, \tag{25}$$

where T represents the total storage duration. Then, defining fidelity as $F = |\langle\psi_{\text{out}}(t)|\psi_{\text{in}}(t - T)\rangle|^2$, one readily obtains

$$F = \left|\int_{-\infty}^{\infty} \mathrm{d}\omega\Gamma(\omega)|f_p(\omega)|^2\right|^2 \Big/ \int_{-\infty}^{\infty} \mathrm{d}\omega|\Gamma(\omega)f_p(\omega)|^2. \tag{26}$$

Fidelity can be optimized independently of QE. Fidelity does not depend on tooth narrowness, in contrast to QE (see equation (21)). Moreover, while QE drops to zero at small optical density, fidelity can approach 100% in the same conditions. Indeed, $\Gamma(\omega) \cong \omega_p\chi''(\omega)L/c$ when $\omega_p\chi''(\omega)L/c \ll 1$ and, provided absorption is uniform over the signal bandwidth, substitution into equation (26) leads to $F \cong 100\%$, which is consistent with recent experimental results [28, 29].

In the extreme opposite conditions of infinite optical density, a situation of interest is offered by symmetric spectral shapes, with $|f_p(\omega)|^2 = |f_p(-\omega)|^2$. Broadband symmetric shapes should indeed be used to make the best of the memory multi-mode capacity. Then, since $\chi'(\omega) = -\chi'(\omega)$, equation (26) reduces to

$$F = \int_{-\infty}^{\infty} \mathrm{d}\omega \frac{|f_{p,s}(\omega)|^2}{\{1 + [\chi'(\omega)/\chi''(\omega)]^2\}}. \tag{27}$$

In this situation, phase mismatching affects fidelity in quite the same way as QE (see equation (22)).

In summary, phase mismatching significantly alters both QE and fidelity of finite-bandwidth AFC QM. In the following section, we propose a method to compensate dispersion effects in order to take better advantage of the AFC bandwidth and of the memory multi-mode capacity.

4. Modified AFC scheme with compensated spectral dispersion

As discussed above, the AFC memory is affected by spectral dispersion. Dispersion leads to superluminal propagation features and to phase mismatching of the retrieved field. Phase mismatching reflects incomplete light-atom reversibility, in contrast with the CRIB scheme [31]. In order to restore reversibility, we propose a MAFC scheme that cancels the dispersion effect.

While fast light features spoil AFC memory reversibility, the opposite slow light effect can also be observed in the context of linear absorption, as discussed [32] and experimentally demonstrated recently [33–35]. Indeed, slow light is not specific to nonlinear processes such as electromagnetically induced transparency, but can also merely result from the existence of a transparency window within an absorption profile. This suggests that we should compensate the AFC superluminal effect by simply inserting the memory comb within the transparent spectral interval between two absorbing lines.

The MAFC principle is sketched in figure 3. The AFC occupies the central part of the absorption profile. A rectangular shape is assigned to the $G_o(\Delta)$ AFC envelope. This function is flat over the Δ_{in}-wide memory bandwidth and drops to zero outside this interval. On the sides of the AFC, the absorption lines $G_s(\Delta + \Delta_o/2)$ and $G_s(\Delta - \Delta_o/2)$ generate the slow light effect that will cancel the fast light feature induced by the AFC. The line centres are separated by interval Δ_o. Spectral hole burning techniques [26, 28, 34, 36] can be used to shape such a complex absorption profile.

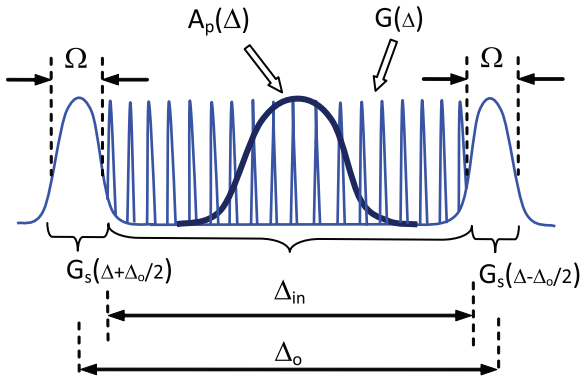

Figure 3. Modified AFC. The AFC is contained between two absorbing lines. Those lines give rise to positive dispersion and the slow light effect that compensates the AFC-induced negative dispersion and the fast light feature.

Let the normalized rectangular AFC envelope be defined as

$$G_o(\Delta) = \begin{cases} \frac{1}{\Delta_{\mathrm{in}}}, |\Delta| < \Delta_{\mathrm{in}}/2 \\ 0\ , |\Delta| > \Delta_{\mathrm{in}}/2. \end{cases} \tag{28}$$

The absorption lines on the sides are given by the following normalized shape:

$$G_s(\Delta \pm \Delta_o/2) = \frac{\Omega}{\pi[(\Delta \pm \Delta_o/2)^2 + \Omega^2]}. \tag{29}$$

Rectangular-shaped AFC was typical in recent experiments [21, 26, 28, 29, 36]. However, the role of the side parts of the absorption profile was not discussed.

We aim at making the real part of susceptibility vanish over the AFC. We rely on two adjustable parameters, namely the relative amplitude f_s of the side lines and their relative spacing $\Delta_o/\Delta_{\mathrm{in}}$, to optimize the suppression of dispersion effects.

One should be aware that the present AFC departs from our assumptions in sections 2 and 3. In those sections, the AFC envelope was represented by a continuous function. Therefore, one could make the optical density arbitrarily large over the entire processing spectral range by increasing the medium thickness L. In the present case, the AFC is sharply cut on the edges. Therefore, signal wings outside the Δ_{in}-wide band are unavoidably lost. Another consequence of the AFC rectangular shape is to invalidate the slowly varying envelope assumption we made in section 2 and especially in equation (8). However, this only affects the very edges of the AFC, over a spectral range of order $b \ll \Delta_{\mathrm{in}}$. Hence, we shall neglect the corresponding error.

Let us examine the signal transmission over the AFC spectral interval $[-\Delta_{\mathrm{in}}/2, \Delta_{\mathrm{in}}/2]$. According to equations (13)–(15), the real and imaginary parts of AFC susceptibility read

$$\chi'_A(\omega) = \frac{c}{\omega_p}\alpha_o \frac{1}{\pi}\mathrm{Ln}\left(\frac{\Delta_{\mathrm{in}}/2 - \omega}{\Delta_{\mathrm{in}}/2 + \omega}\right) \tag{30}$$

$$\chi''_A(\omega) = -\frac{c}{\omega_p}\alpha_o, \tag{31}$$

where

$$\alpha_o = 2\pi \frac{\beta g}{\Delta_{\mathrm{in}}} \frac{1}{\kappa(0)\delta}. \tag{32}$$

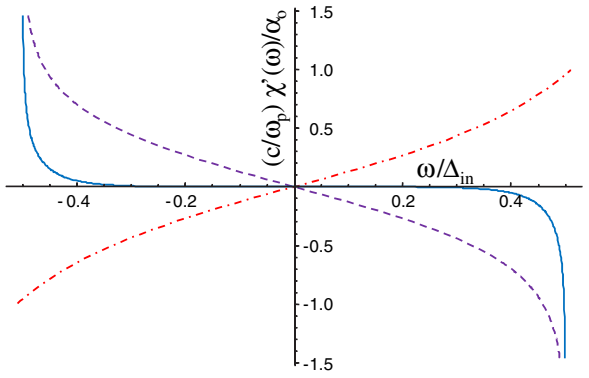

Figure 4. Variations of $\chi'_A(\omega)$ (dashed line), $\chi'_s(\omega)$ (dash-dotted line) and $\chi'_M(\omega)$ (solid line) over the AFC spectral range. The AFC fast light effect (negative dispersion) is compensated by the slow light effect (positive dispersion) induced by the side lines.

Under assumption $\Omega \ll \Delta_o - \Delta_{\text{in}}$, the side lines stay outside the AFC. Residual absorption by those lines at the AFC centre is expressed by the absorption coefficient

$$\alpha_s(0) = 4 f_s \frac{\beta g \Omega}{(\Delta_o/2)^2}. \tag{33}$$

This does not affect the signal round trip through the AFC medium provided

$$\frac{2\alpha_s(0)}{\alpha_o} = \frac{4}{\pi} f_s \kappa(0) \delta \frac{\Omega \Delta_{\text{in}}}{(\Delta_o/2)^2} \ll 1. \tag{34}$$

As for the real part of susceptibility, the side lines bring the contribution

$$\chi'_s(\omega) = \frac{c}{\omega_p} \alpha_o \frac{1}{\pi} f_s \kappa(0) \delta \frac{2\omega \Delta_{\text{in}}}{(\Delta_o/2)^2 - \omega^2} \tag{35}$$

over the AFC range, where $\Omega \ll \Delta_o/2 - |\omega|$. The real part of MAFC susceptibility reads $\chi'_M(\omega) = \chi'_A(\omega) + \chi'_s(\omega)$ and vanishes to third-order expansion of equations (30), (35) in $\omega/\Delta_{\text{in}}$, provided the following relations are satisfied:

$$\Delta_o = \sqrt{3}\Delta_{\text{in}}, \quad f_s \kappa(0) \delta = \tfrac{3}{2}. \tag{36}$$

The spectral variations of $\chi'_A(\omega)$, $\chi'_s(\omega)$ and $\chi'_M(\omega)$ are displayed in figure 4, showing the compensation of AFC fast light by the slow light effect from the side lines. As a result, in the $\alpha_o L \gg 1$ large optical density limit, the efficiency factor $|\Gamma(\omega)|^2$ of the MAFC gets close to unity over the entire AFC bandwidth, unlike the original AFC scheme, as illustrated in figure 5.

Dispersion cancellation impacts on QE and fidelity, as illustrated in figure 6. In this figure, the incoming signal is assigned a Gaussian spectrum, centred at the middle of the AFC band and the optical density is assumed to be large. As discussed in section 3.2, QE and fidelity are expressed by the same number in this situation. Unlike conventional AFC parameters, MAFC QE and fidelity keep very close to an ideal process, with complete elimination of dispersion. However, as pointed out above, both QE and fidelity suffer from the loss of spectral components lying outside the AFC processing band, even when dispersion effects completely cancel.

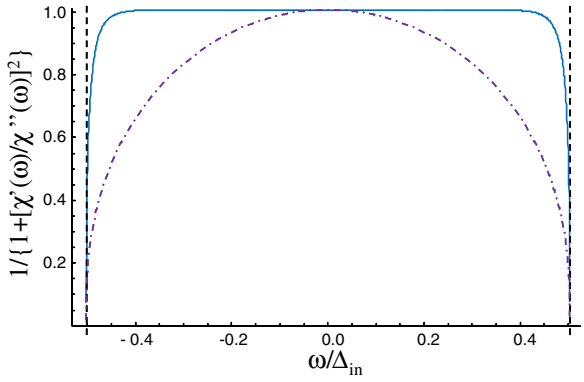

Figure 5. AFC (dash-dotted line) and MAFC (solid line) spectral distribution of $1/\left(1 + [\chi'(\omega)/\chi''(\omega)]^2\right)$ over the AFC bandwidth.

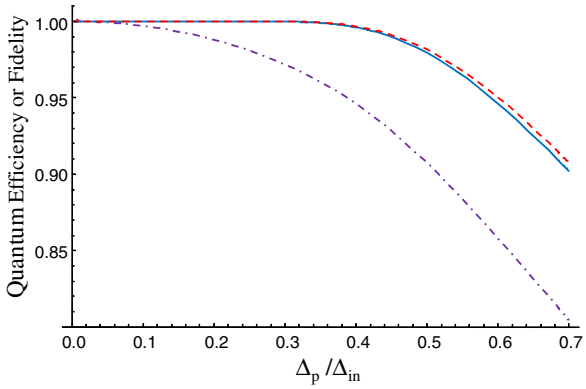

Figure 6. Gaussian signal recovery. QE and/or fidelity are displayed as a function of the signal spectrum FWHM, normalized to the AFC bandwidth. AFC (dash-dotted line) and MAFC (solid line) expected accomplishments are displayed together with a perfect operation result (dotted line), with complete elimination of dispersion.

5. Discussion and conclusion

Infinite bandwidth, AFC-based, quantum memory (QM) may offer 100% quantum efficiency (QE) and fidelity when the signal is retrieved in the backward direction. This is no longer true when the memory spectral width is limited. Since the dispersive part of susceptibility no longer vanishes, the retrieved signal is no longer spatially phase matched to the atomic coherences. In contrast with CRIB, the mismatching accumulated during the storage step is not compensated during the recovery stage, which reveals the intrinsic non-reversibility of AFC.

After demonstrating these features, we have proposed a modified AFC (MAFC) scheme that restores spatial phase matching and reversibility. By setting absorption lines on the sides of the AFC, we reduce the group velocity. Hence, the superluminal effect caused by the AFC itself is cancelled by a slow light effect.

One may wonder whether MAFC generates a significant gain in memory bandwidth. This question arises if one assumes that the AFC can be etched over all the available inhomogeneous width. Indeed, about half of this available width is wasted by implementing the MAFC. The net gain in bandwidth at 90% QE appears to be small. However, one should be aware that much higher QE is required for quantum computing applications [37]. In addition, engraving

a high-efficiency AFC, with large average optical depth, is a difficult challenge, as testified by the actual experimental achievements. In existing demonstrations, the AFC has been etched over the narrowest possible range, hardly exceeding the signal bandwidth. In this context, the MAFC makes sense.

The analysis and the method to cure non-reversibility could be extended to recently proposed photon echo [23–25] or Raman echo [17, 38–41] QM schemes based on persistent inhomogeneous broadening.

Acknowledgments

SAM would like to thank Université Paris Sud for supporting his visit to Laboratoire Aimé Cotton and for the hospitality shown to him during his visit. SAM also acknowledges the support from the Russian Foundation for Basic Research through grant no. 10-02-01348.

References

[1] Hahn E 1950 *Phys. Rev.* **80** 580
[2] Kopvil'em U and Nagibarov V 1963 *Fiz. Met. Metalloved.* **2** 313 (in Russian)
[3] Kurnit N A, Abella I D and Hartmann S R 1964 *Phys. Rev. Lett.* **13** 567
[4] Fernbach S and Proctor W 1955 *J. Appl. Phys.* **26** 170
[5] Elyutin S O, Zakharov S M and Manykin E A 1979 *Sov. Phys.—JETP* **49** 421
Elyutin S O, Zakharov S M and Manykin E A 1979 *Zh. Eksp. Teor. Fiz.* **76** 835–45
[6] Zuikov V A, Samartsev V V and Usmanov R G 1980 *JETP Lett.* **32** 270
Zuikov V A, Samartsev V V and Usmanov R G 1980 *Pis. Zh. Eksp. Teor. Fiz.* **32** 293
[7] Mossberg T 1982 *Opt. Lett.* **7** 77
[8] Lvovsky A I, Sanders B C and Tittel W 2009 *Nature Photon.* **3** 706
[9] Tittel W, Afzelius M, Chanelière T, Cone R L, Kröll S, Moiseev S A and Sellars M 2010 *Laser Photon. Rev.* **4** 244
[10] Simon C *et al* 2010 *Eur. Phys. J.* D **58** 1
[11] Moiseev S A and Kröll S 2001 *Phys. Rev. Lett.* **87** 173601
[12] Moiseev S A, Tarasov V F and Ham B S 2003 *J. Opt. B: Quantum Semiclass. Opt.* **5** 497
[13] Nilsson M and Kroll S 2005 *Opt. Commun.* **247** 393
[14] Kraus B, Tittel W, Gisin N, Nilsson M, Kröll S and Cirac J I 2006 *Phys. Rev.* A **73** 020302
[15] Alexander A L, Longdell J J, Sellars M J and Manson N B 2006 *Phys. Rev. Lett.* **96** 043602
[16] Hétet G, Longdell J J, Alexander A L, Lam P K and Sellars M J 2008 *Phys. Rev. Lett.* **100** 023601
[17] Hétet G, Hosseini M, Sparkes B M, Oblak D, Lam P K and Buchler B C 2008 *Opt. Lett.* **33** 2323
[18] Hedges M P, Longdell J J, Li Y and Sellars M J 2010 *Nature* **465** 1052
[19] Hosseini M, Sparkes B M, Lam P and Buchler B 2011 *Nature Commun.* **2** 174
[20] Moiseev S A and Arslanov N M 2008 *Phys. Rev.* A **78** 023803
[21] de Riedmatten H, Afzelius M, Staudt M U, Simon C and Gisin N 2008 *Nature* **456** 773
[22] Afzelius M, Simon C, de Riedmatten H and Gisin N 2009 *Phys. Rev.* A **79** 052329
[23] Moiseev S A 2011 *Phys. Rev.* A **83** 012307
[24] McAuslan D L, Ledingham P M, Naylor W R, Beavan S E, Hedges M P, Sellars M J and Longdell J J 2011 *Phys. Rev.* A **84** 022309
[25] Damon V, Bonarota M, Louchet-Chauvet A, Chanelière T and Le Gouët J-L 2011 *New J. Phys.* **13** 093031
[26] Usmani I, Afzelius M, de Riedmatten H and Gisin N 2010 *Nature Commun.* **1** 12
[27] Bonarota M, Le Gouët J L and Chanelière T 2011 *New J. Phys.* **13** 013013
[28] Clausen C, Usmani I, Bussières F, Sangouard N, Afzelius M, de Riedmatten H and Gisin N 2011 *Nature* **469** 508
[29] Saglamyurek E, Sinclair N, Jin J, Slater J A, Oblak D, Bussières F, George M, Ricken R, Sohler W and Tittel W 2011 *Nature* **469** 512
[30] Wang L, Kuzmich A and Dogariu A 2000 *Nature* **406** 277
[31] Moiseev S A and Noskov M I 2004 *Laser Phys. Lett.* **1** 303
[32] Shakhmuratov R N, Rebane A, Mégret P and Odeurs J 2005 *Phys. Rev.* A **71** 053811
[33] Camacho R M, Pack M V and Howell J C 2006 *Phys. Rev.* A **74** 033801
[34] Lauro R, Chanelière T and Le Gouët J-L 2009 *Phys. Rev.* A **79** 063844
[35] Walther A, Amari A, Kröll S and Kalachev A 2009 *Phys. Rev.* A **80** 012317
[36] Bonarota M, Ruggiero J, Le Gouët J-L and Chanelière T 2010 *Phys. Rev.* A **81** 033803
[37] Knill E 2005 *Nature* **434** 39
[38] Nunn J, Reim K, Lee K C, Lorenz V O, Sussman B J, Walmsley I A and Jaksch D 2008 *Phys. Rev. Lett.* **101** 260502
[39] Le Gouët J-L and Berman P R 2009 *Phys. Rev.* A **80** 012320
[40] Hosseini M, Sparkes B M, Hétet G, Longdell J, Lam P and Buchler B 2009 *Nature* **461** 241
[41] Moiseev S and Tittel W 2011 *New J. Phys.* **13** 063035